ACS Catalysis

Research Article

Cite This: ACS Catal. 2019, 9, 8509−8519

pubs.acs.org/acscatalysis

A Hydrophilic Channel Is Involved in Oxidative Inactivation of a [NiFeSe] Hydrogenase

Sónia Zacarias,[†] Adriana Temporão,[†] Melisa del Barrio,[‡] Vincent Fourmond,[‡] Christophe Léger,[‡] Pedro M. Matias,*[,†,§] and Inês A. C. Pereira*[,†]

[†]Instituto de Tecnologia Química e Biológica António Xavier, Universidade Nova de Lisboa, Av. da República, 2780-157 Oeiras, Portugal

[‡]Aix Marseille Univ., CNRS, Bioénergétique et Ingénierie des Protéines, UMR 7281 Marseille, France

[§]iBET, Instituto de Biologia Experimental e Tecnológica, Apartado 12, 2780-901 Oeiras, Portugal

Supporting Information

ABSTRACT: Hydrogenases are metalloenzymes that catalyze the redox conversion between H_2 and protons. The so-called [NiFeSe] hydrogenases are highly active for both H_2 production and oxidation, but like all hydrogenases, they are inhibited by O_2. In the [NiFeSe] enzyme from *Desulfovibrio vulgaris* Hildenborough this inhibition results from the oxidation of an active site cysteine ligand. We designed mutations that constrict a hydrophilic channel which connects the protein surface to this active site cysteine. Two of the variants show markedly increased tolerance to O_2 inactivation, while they retain high catalytic activities in both directions of the reaction, and structural studies confirm that these mutations prevent the oxidation of the cysteine. Our results indicate that the diffusion of O_2 or ROS to the active site can occur through a hydrophilic water channel, in contrast to the widely held assumption that only hydrophobic channels are involved in active site inactivation. This provides an original strategy for optimizing the enzyme by protein engineering.

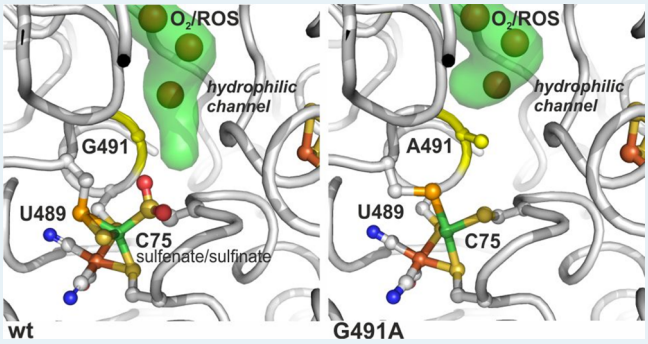

KEYWORDS: *hydrogen, hydrogenases, selenium, hydrophilic channel, sulfenate, sulfinate*

INTRODUCTION

Hydrogenases are extremely efficient biocatalysts for H_2 production and oxidation, which use only earth-abundant transition metals as cofactors. The study of these enzymes and their catalytic mechanism may lead to important insights in the efforts to develop an H_2-based economy.[1] However, most hydrogenases are sensitive to O_2, which hampers their use in large-scale applications. Thus, understanding and preventing the inhibition of hydrogenases by O_2 is of major interest, as it could crucially influence the applicability of these enzymes as efficient catalysts in an H_2-fueled economy.

The most common hydrogenases are the [NiFe] and the [FeFe] hydrogenases, so named on the basis of the active site metal content.[1] In both classes, this active site is deeply buried inside the protein and a network of hydrophobic channels guides the diffusion of substrate H_2 and inhibitors, such as O_2 and CO, between the solvent and the active site.[2−10] Most [FeFe] hydrogenases are slowly but irreversibly damaged by O_2.[10] The inactivation of the so-called "standard" [NiFe] hydrogenases involves the formation of a mixture of two EPR-detectable inactive states where an oxygen species bridges the active site metal ions; the two inactive states can be reactivated by reduction, albeit at very different rates.[11−13] The [NiFeSe] hydrogenases are a subclass of the [NiFe] hydrogenases, where a selenocysteine (Sec) replaces cysteine as one of the nickel terminal ligands (Figure S1).[14,15] Two [NiFeSe] hydrogenases have been studied in detail, those from *Desulfomicrobium baculatum*[16] and *Desulfovibrio vulgaris* Hildenborough.[17] Both exhibit very high catalytic activities,[17−19] and the *Dm. baculatum* enzyme was shown to be less inhibited by H_2 and O_2 than the [NiFe] counterparts, which results in the ability to produce H_2 under low levels of O_2.[19−21] The active site Sec ligand of the *D. vulgaris* Hildenborough [NiFeSe] hydrogenase was observed to play a key role in its high activity and oxygen tolerance,[18] but other features are also relevant. These include a "cage effect" observed through experimental data and predicted by theoretical calculations, enabling a high H_2 density near the active site,[22−24] and differences in the proton transfer pathways and H_2 channels.[22] [NiFeSe] hydrogenases are inactivated in the presence of high O_2 concentrations, but they can be quickly reactivated by reduction,[19,25] probably because of the reversible reactivity of Sec with O_2.[26] An

Received: June 5, 2019
Revised: July 23, 2019
Published: August 5, 2019

DOI: 10.1021/acscatal.9b02347
ACS Catal. 2019, 9, 8509−8519

exogenous sulfur atom bound to Ni, observed in the structure of *D. vulgaris* Hildenborough [NiFeSe] hydrogenase (Figure S1), may also play a role by preventing the formation of inactive species where an oxide bridges the two metal ions.[18,27] Nevertheless, oxygen damage has been observed in the crystal structures of both [NiFeSe] hydrogenases. In the aerobically isolated enzyme from *D. vulgaris* Hildenborough the proximal iron−sulfur cluster is reversibly modified by the binding of two oxygen atoms, and the terminal Ni ligand, Cys75 (large subunit), is irreversibly oxidized to sulfinate.[27] In addition, the sulfur species at the active site causes the side chain of Sec489 to be present in three possible conformations, named I, II, and III (Figure S1), where conformer III corresponds to that found in the active reduced form of the [NiFe] and [NiFeSe] hydrogenases.[27,28] In the [NiFeSe] hydrogenase from *Dm. baculatum*, the crystal structure of the enzyme purified aerobically displayed a complex mixture of oxidized states.[29] Some of these could be resolved only when the enzyme was purified anaerobically, showing a mixture of three oxidized states, including seleninate and selenate species and an additional oxygen or sulfur atom bridging the Ni and Fe ions. Despite the structural similarity between the two [NiFeSe] hydrogenases,[28,30] the available data indicate that the effects of O_2 inactivation are quite enzyme specific.[27,29] Nevertheless, it should be noted that the experimental conditions used to expose both enzymes to O_2 were different.

Recently, we developed a system for recombinant expression of a soluble form of the [NiFeSe] hydrogenase from *D. vulgaris* Hildenborough,[18] allowing the production of stable and abundant protein with high H_2 production and oxidation activities.[18,31] The recombinant enzyme has been applied in optimized biofuel cells, which show benchmark open circuit voltages and current densities for H_2 oxidation.[32−34] Its high H_2 production activity makes this enzyme attractive for photochemical H_2 production[35] and other applications such as electrochemical ATP synthesis.[36]

The engineering of a [NiFeSe] hydrogenase to improve its O_2 tolerance has not been reported before. Here, we used rational design to prevent the irreversible oxidation of Cys75. The mechanism of Cys75 oxidation probably involves a reaction with reactive oxygen species (ROS),[37] which may be formed close to the active site by reduction of O_2. However, Cys75 is not directly accessible via the hydrophobic channel through which O_2 molecules are proposed to diffuse.[2−9] It is possible that the oxidation of Cys75 may arise due to its location at the end of a water channel leading to the protein surface, which is only found in the crystal structures of [NiFeSe] hydrogenases (Figure 1). However, this channel is hydrophilic and, as a nonpolar molecule, O_2 is expected to diffuse instead through the hydrophobic channels;[2] therefore, evidence for O_2 diffusion through this water channel would be unprecedented for hydrogenases. We examined the effects of replacing two residues that line this hydrophilic channel, Gly50, located near the protein surface, and Gly491, which is near Cys75. We observed that mutations G491A and G491S prevent, or considerably slow, the oxidation of Cys75, resulting in more oxygen tolerant variants and demonstrating the role of this solvent channel in providing access of O_2 or ROS to the active site in the *D. vulgaris* Hildenborough [NiFeSe] hydrogenase.

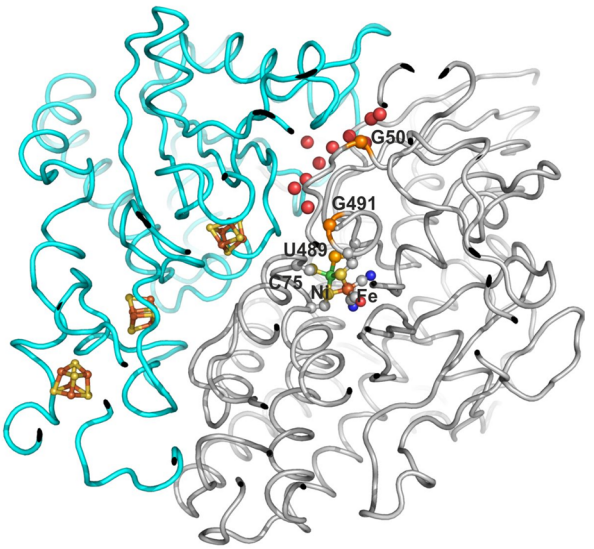

Figure 1. Solvent channel in the 0.95 Å resolution structure of the anaerobically crystallized wild-type [NiFeSe] hydrogenase from *D. vulgaris* Hildenborough (PDB 5JSH). The protein Cα backbone is shown in light cyan for the small subunit and gray for the large subunit, the water molecules in the solvent channel are shown as red spheres, the active site and the iron−sulfur clusters are depicted in ball-and-stick representation with atom colors gray for carbon, blue for nitrogen, red for oxygen, gold for sulfur, and brown for iron, and the G50 and G491 residues are highlighted in orange.

RESULTS

Rational Design of [NiFeSe] Hydrogenase Variants. On the basis of a structural alignment between the *D. vulgaris* Hildenborough [NiFeSe] hydrogenase and other members of the [NiFe] hydrogenase family (Figure S2) we selected two residues in the large subunit of the [NiFeSe] enzyme, which are in a solvent channel linking Cys75 to the protein surface (Figure 1). Gly50 is near the protein surface at ca. 15 Å from the Ni atom in the active site, whereas Gly491 is very close to the active site at a distance of ca. 6 Å from the same atom. In [NiFe] hydrogenases, Gly50 and Gly491 are replaced with threonine or glutamine and alanine or serine, respectively; thus, a similar channel does not exist. With the aim of blocking the putative solvent channel leading directly to Cys75 and trying to prevent its oxidation, we generated the G50T and G491A variants, which reproduce the sequence of standard [NiFe] hydrogenases. We also produced the G491S, G491T, and G491V variants, to test the effects of side chain polarity and size at position 491.

Kinetic and Structural Characterization of the [NiFeSe] Hydrogenase Variants. Variants G50T, G491A, and G491S were successfully purified and characterized. However, no stable protein could be obtained for the G491T and G491V variants. Although threonine and valine are not bulky residues, the additional carbon atom at position 491 may induce a steric disruption. The G50T, G491A, and G491S mutations moderately decreased the H_2 production and oxidation activities of the enzyme (Table 1), but the turnover frequencies remained near or above 3000 s^{-1}, which is high in the context of [NiFe] hydrogenases. All variants retain a catalytic bias toward H_2 production in the solution assays.

Crystal structures of the G50T, G491A, and G491S variants were obtained under aerobic conditions at resolutions of 1.10, 1.36, and 1.20 Å, respectively (Tables S1 and S2). The

DOI: 10.1021/acscatal.9b02347
ACS Catal. 2019, 9, 8509−8519

Table 1. Turnover Rate (s^{-1}) for *D. vulgaris* Hildenborough [NiFeSe] Hydrogenase and Variants[a]

	WT	G491A	G491S	G50T
H_2 evolution	8270 ± 380[b]	6020 ± 100	3510 ± 140	3820 ± 210
H_2 uptake	4850 ± 260	4080 ± 80	2810 ± 150	nd

[a]Turnover rate for H_2 production at 37 °C in 50 mM Tris-HCl buffer at pH 7 with 1 mM MV reduced with 15 mM sodium dithionite. Turnover rate for H_2 oxidation under 0.5 bar H_2, at 30 °C, in 50 mM Tris/HCl pH 8 containing 2 mM of MV. nd = not determined. [b]From ref 18.

previously reported 1.30 Å structure of the recombinant WT [NiFeSe] hydrogenase in the as-isolated, oxidized form (PDB 5JSH) is used for comparison.[18] No changes are observed in the overall protein structures, relative to the WT. The structural analysis of the variants will focus on the oxidative modification of the active site (Table S3), namely in the relative abundance of the three different Sec conformations (Figure S1) and degree of oxidation of Cys75 to sulfenate and sulfinate.

In the G50T crystal structure, Sec489 displays conformers I, II, and III with occupancies of 46%, 20%, and 34% (Figure S3A,B), similar to those previously reported for the WT structure (52%, 20%, and 29% respectively). In the G491A structure only Sec489 conformers II and III are observed with occupancies of 23% and 77%, respectively, indicating that this residue is mainly in the active, reduced conformation (Figure 2). Finally in the G491S structure, conformers I, II, and III are

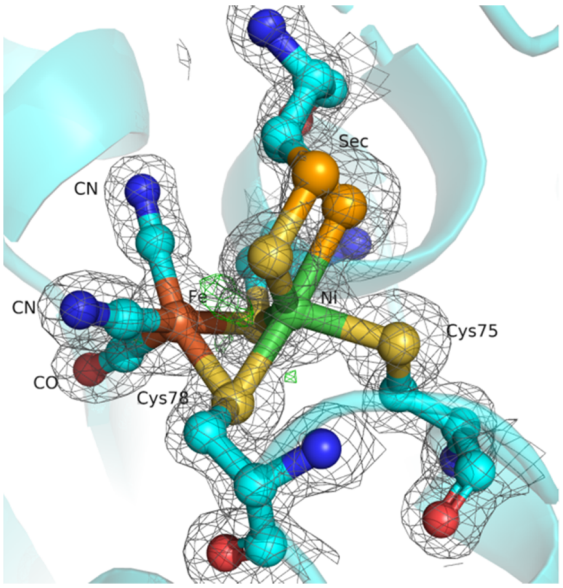

Figure 2. Active site surroundings in the crystal structure of the aerobically purified and crystallized G491A [NiFeSe] hydrogenase variant and its corresponding $2|F_o| - |F_c|$ (gray mesh, 1.5 map rms) and $|F_o| - |F_c|$ (green mesh, 3.5 map rms) maps. No negative peaks are visible at −3.5 rms in the $|F_o| - |F_c|$ map. Atoms are color-coded as follows: brown, Fe; green, Ni; gold, S; red, O; light blue, C; blue, N; orange, Se. H atoms are omitted for clarity.

present with occupancies of 29%, 18%, and 53%, respectively, with Sec489 still predominantly in the active conformation (Figure S3C,D). In the G50T structure, the terminal Cys75 Ni ligand is extensively oxidized to the sulfenate (20%) and sulfinate (54%) states, similarly to the WT (38% and 62%, respectively). Thus, the G50T mutation has no significant effect on the oxidized state of the active site. In contrast, in the G491A structure, Cys75 is not oxidized at all (Figure 2), and in the G491S structure it is only slightly oxidized to the sulfinate state (ca. 20%) (Figure S3C,D). These results are a clear indication that the G491 mutations protect Cys75 from oxidative modification. Furthermore, the G491S variant shows reduced oxygenation of the proximal cluster (Table S3), raising the possibility that this mutation may also reduce access of ROS/O_2 to this cluster.

Electrochemical Studies of O_2 and CO Inhibition. The (in)activation of NiFeSe hydrogenase in response to changes in O_2 concentration or redox conditions has been studied by electrochemistry,[19,25] in experiments where electron transfer between the enzyme and the electrode is direct and the turnover frequency is measured as a current.[38,39] In particular, we have shown that *D. vulgaris* Hildenborough [NiFeSe] hydrogenase is inactivated either in the presence of O_2 or at high electrode potential to inactive states that can be reduced when the electrode potential is swept down. The potential where reactivation occurs in voltammetric experiments strongly depends on the scan rate, because the rate of reactivation increases as the electrode potential decreases,[25] as occurs with all [NiFe] and [FeFe] hydrogenases characterized so far. Here we focus on the kinetics of inactivation by O_2. The experiment consists in measuring the hydrogen oxidation current (which is proportional to turnover rate) and examining the effect of injecting a small volume of air-saturated buffer solution (containing 240 μM O_2) into the electrochemical cell, to reach 0.5 μM O_2. The O_2 concentration increases instantly at the time of injection and then decreases exponentially over time, as the dissolved O_2 is flushed out of the cell by the stream of H_2. We perform these experiments at high electrode potential to prevent the direct reduction of O_2 on the electrode, which would contribute to the current, decrease the concentration of O_2 that the enzyme experiences, and produce reactive oxygen species.[40] The changes in H_2 oxidation current obtained for the WT enzyme and variants are shown in Figure 3. When O_2 is introduced (at 175 s in the figure), the activity of the WT and G50T variant quickly vanishes, whereas, all things being equal, the G491S and G491A variants are slowly and only partially inactivated. The initial decrease in current, before O_2 addition, is due to enzyme desorption and anaerobic oxidative inactivation[41] and was corrected by assuming that the loss of current follows first-order kinetics. The inactivation rate constants were determined by fitting to the data a model that assumes that the enzyme inactivates in an oxygen-dependent reaction (second-order rate constant $k_{in}^{O_2}$), followed by either reactivation (first-order rate constant k_a) or irreversible inactivation (k_3):[42]

$$A \underset{k_a}{\overset{k_{in}^{O_2}[O_2]}{\rightleftharpoons}} I \xrightarrow{k_3} D \quad (1)$$

In this scheme, A represents the active species, I the inactive species, and D the dead-end species formed by irreversible inactivation.

The best values of the inactivation and reactivation rate constants are given in Table 2. At the potential used, we observed a very slow reactivation ($k_a \approx 10^{-4}$ s^{-1}) for all four

DOI: 10.1021/acscatal.9b02347
ACS Catal. 2019, 9, 8509−8519

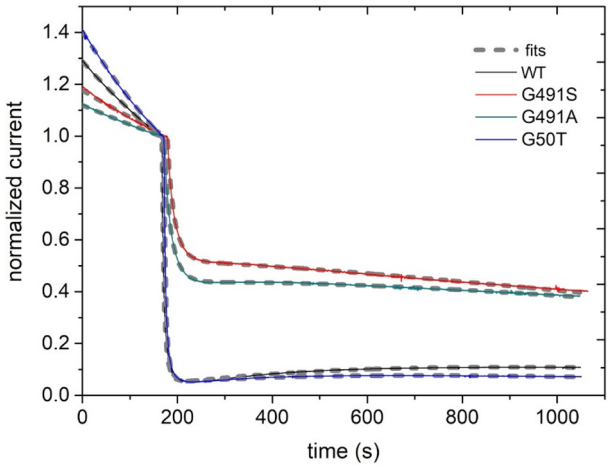

Figure 3. Effect of O_2 on the H_2 oxidation current of WT [NiFeSe] hydrogenase and variants adsorbed onto a graphite rotating electrode. The gray dashed lines are the best fits of the kinetic model in eq 1. Experimental conditions: $[O_2]$ = 0.5 μM, E = 0.14 V vs SHE, 1 bar H_2, pH 7, T = 40 °C, electrode rotation rate 3000 rpm.

enzymes. The k_3 rate constants were small (possibly zero) and could not be determined accurately. The values of $k_{in}^{O_2}$ in Table 2 demonstrate that the two G491 mutations decrease the rate of inactivation by O_2 about 7-fold.

In [NiFe] hydrogenases, it is believed that both CO and O_2 access the active site through the same gate at the end of a hydrophobic gas channel, and it was found that the rate of CO inhibition is a good proxy for the rate of intramolecular diffusion of other gases to the active site.[7] We evaluated the rates of inhibition by CO (k_{in}^{CO}) and the rate of CO release (k_{out}^{CO}) for the WT and the variants by monitoring the H_2 oxidation current after exposure to CO at −60 mV and 40 °C (Figure S6). In all cases, the current decreases upon CO injection and then recovers its initial value as CO is flushed away from the solution, showing that the enzymes are reversibly inhibited by CO. To determine the constants of CO inhibition, we fitted to the data a model that assumes bimolecular CO binding to the active and first-order kinetics for CO release:[5]

$$\mathrm{E} \underset{k_{out}}{\overset{k_{in}[\mathrm{CO}]}{\rightleftharpoons}} \mathrm{ECO} \qquad (2)$$

Since CO inhibition of [NiFe] hydrogenases is competitive[40] the measured rate constant of CO binding is not the true rate but is multiplied by $K_m/(K_m + [H_2])$.[7,43] This does not matter here for comparison of the rates, since we have not observed any effect of the mutations on the Michaelis constant for H_2. In contrast to what we observed with O_2, all four enzymes react with CO at about the same rate.

Effect of O_2 Exposure on H_2 Uptake Activity in Solution. To study the effect of prolonged air exposure and the reversibility of oxidative damage, we first activated each enzyme with H_2 and then exposed it to air for 1 h, 4 h, or overnight (ca. 16 h) at room temperature. After exposure to air, no activity was detected in either the WT or variants, consistent with previous evidence that reactivation requires that the enzyme be reduced.[19,25] The inactive samples were then incubated under H_2 for 10, 30, or 90 min, before measuring how much activity remained or was irreversibly lost. The G50T variant was not tested in this experiment, since the structural and electrochemical data indicated no significant difference from the WT.

For the WT enzyme we observed that, after 1 h exposure to air and reactivation with H_2, the enzyme loses 30% of the initial activity. The loss in activity increases with exposure time, reaching 50% after overnight exposure to air (Figure 4). In

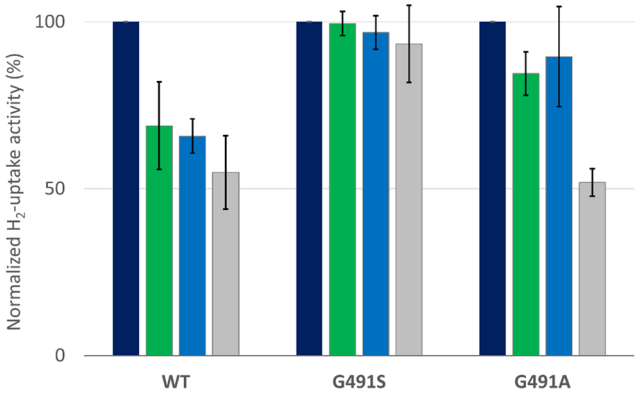

Figure 4. H_2 uptake activity of WT and variants after 1 h (green), 4 h (blue), and 16 h (gray) exposure to air, followed by a 30 min reactivation under 0.5 atm of H_2. The activities were normalized by the corresponding maximum activity of each protein (dark blue), reported in Table 1. Each experiment was performed three times (technical replicates), and the error bars show the corresponding standard deviations.

contrast, the G491S variant is more tolerant to O_2, since even after overnight air exposure (followed by reduction), the activity was not significantly affected. The G491A variant is less sensitive than the WT during the first hours, but overnight air exposure results in a similar loss of activity, by about 50%. The duration of the incubation under H_2 made no difference (Figure S4), with 10 min being enough to reactivate all the proteins. The different behavior between the G491S and G491A variants and the WT suggests that this mutation prevents, or at least considerably delays, the formation of inactive species that do not reactivate. This experiment also emphasizes the robust catalytic behavior of the [NiFeSe] hydrogenase, since the turnovers for WT and variants are all

Table 2. | Kinetic Properties of the *D. vulgaris* Hildenborough [NiFeSe] Hydrogenase WT and Variants

	$k_{in}^{O_2}$ (mM^{-1} s^{-1})[a]	$k_{out}^{O_2}$ (s^{-1})[a]	$^{app}k_{in}^{CO}$ (mM^{-1} s^{-1})[b]	k_{out}^{CO} (s^{-1})[b]
WT	527 ± 10	(3 ± 1) × 10^{-4}	290 ± 50	0.3 ± 0.1
G50T	629 ± 260	(3 ± 0.1) × 10^{-4}	410 ± 220	0.8 ± 0.5
G491A	77 ± 15	(6 ± 2) × 10^{-4}	380 ± 80	0.9 ± 0.4
G491S	86 ± 15	(8 ± 3) × 10^{-4}	400 ± 170	1.0 ± 0.1

[a]Conditions: E = 0.14 V vs SHE, 1 bar H_2, pH 7, T = 40 °C, $[O_2]$ = 0.5 μM. [b]Conditions: E = −0.06 V vs SHE, 1 bar H_2, pH 7, T = 40 °C, [CO] = 1, 2, 4 μM.

DOI: 10.1021/acscatal.9b02347
ACS Catal. 2019, 9, 8509−8519

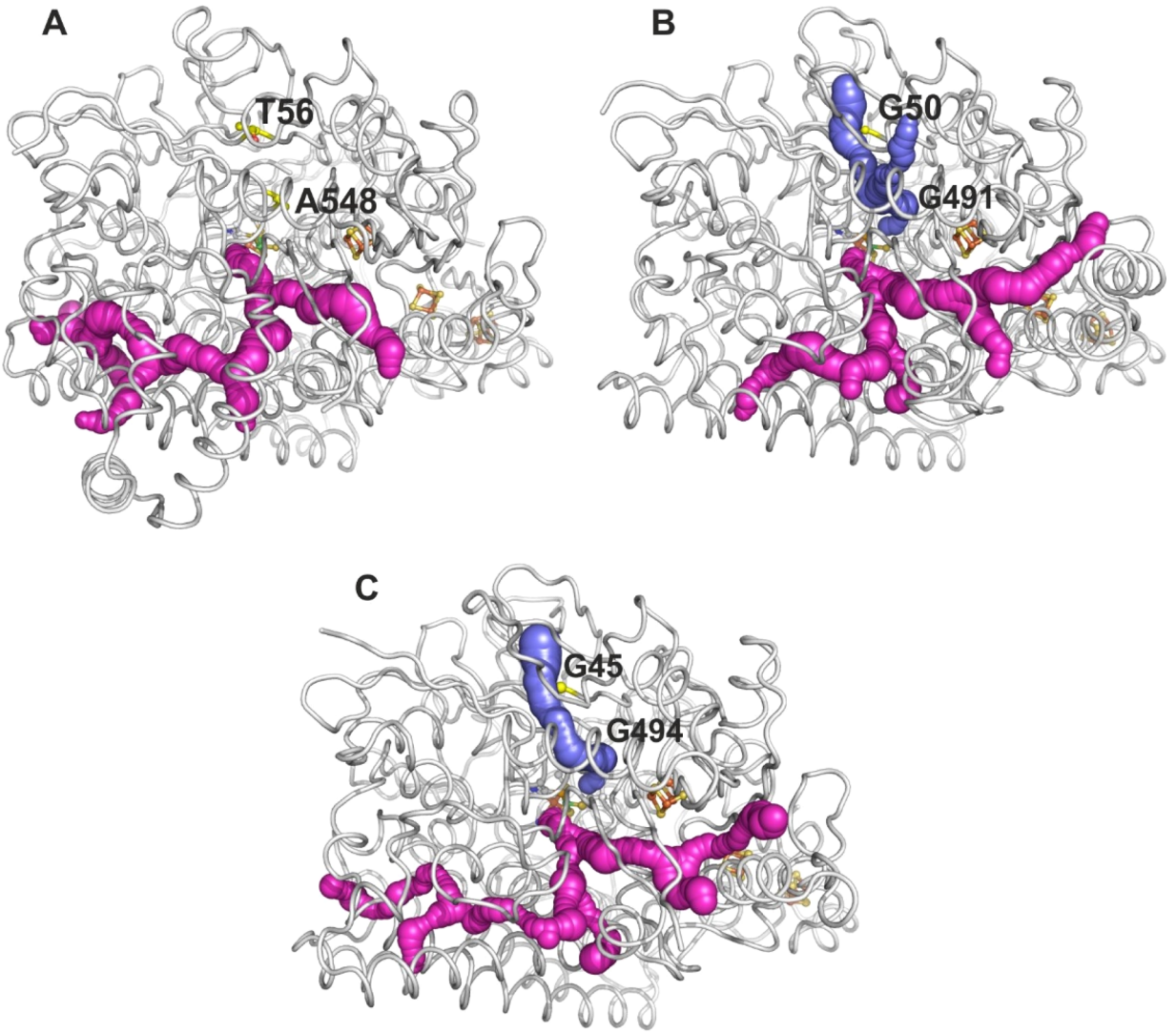

Figure 5. Channels in the high-resolution structures of [NiFe] hydrogenase from *D. vulgaris* Myiazaki F (A, 0.86 Å, PDB 489H), [NiFeSe] hydrogenases from *D. vulgaris* Hildenborough (B, 0.95 Å, PDB 5JSK, crystallized anaerobically), and *Dm. baculatum* (C, 1.4 Å, PDB 4KN9), calculated with CAVER. The hydrophobic channel system allowing H_2 exchange with the active site is shown in light magenta, and the channels connecting Sec and Cys75 Sγ atoms with the enzyme exterior are displayed in blue. The protein Cα backbones are shown as gray tubes; the active site and the iron−sulfur clusters are shown in ball-and-stick representation with atom colors gray for carbon, blue for nitrogen, red for oxygen, gold for sulfur, and brown for iron; the G50 and G491 residues in *D. vulgaris* Hildenborough and their structurally equivalent Thr56 and Ala548 residues in *D. vulgaris* Myiazaki F and G45 and G494 in *Dm. baculatum* are displayed in ball-and-stick representation with carbon atoms colored yellow. For clarity, only the side chains of the protein residues are shown.

above 1000 s^{-1} even after overnight air exposure and reactivation, which is a very high activity in comparison to most [NiFe] hydrogenases.

Structural Analysis of the [NiFeSe] Hydrogenase Channels. We used the software CAVER[44] to analyze and compare the shapes of the channels in the WT *D. vulgaris* Hildenborough [NiFeSe] hydrogenase,[18] in the variants obtained in this work, in the *Dm. baculatum* [NiFeSe] hydrogenase,[29] and in the standard [NiFe] hydrogenases given in Figure S2. Hydrogen atoms were added to the analyzed structures, whenever necessary, using the PHENIX *phenix.ready_set* tool.[45] The *D. vulgaris* Myiazaki F [NiFe] hydrogenase[46] is shown as representative of the results obtained. As illustrated in Figure 5 and previously described,[2] both [NiFe] and [NiFeSe] hydrogenases contain a branched hydrophobic channel system through which H_2 and other small gas molecules diffuse to/from the active site.[8,9] A second channel system is present in both [NiFeSe] hydrogenases, linking the Ni terminal ligands Sec489 and Cys75 (*D. vulgaris* Hildenborough numbering) to the protein surface (Figure 5B,C). CAVER calculations revealed that this channel is not present in the [NiFe] hydrogenases analyzed (Figure 5 and Table S4), here represented by the *D. vulgaris* Myiazaki F [NiFe] hydrogenase (Figure 5A). In the *D. vulgaris* Hildenborough [NiFeSe] hydrogenase, this second channel has a hydrophilic character, starts from the active site, and then divides into two branches (Figures 5B and 6A); the first branch continues the initial hydrophilic segment, while the second is lined by hydrophobic residues and is absent in the [NiFeSe] hydrogenase from *Dm. baculatum* (Figure 5C).

The G50T mutation is located after the branching point, near the end of the hydrophilic branch closer to the surface, while the G491A and G491S mutations are in the first segment of the hydrophilic channel, before the branching point. Figure

DOI: 10.1021/acscatal.9b02347
ACS Catal. 2019, 9, 8509−8519

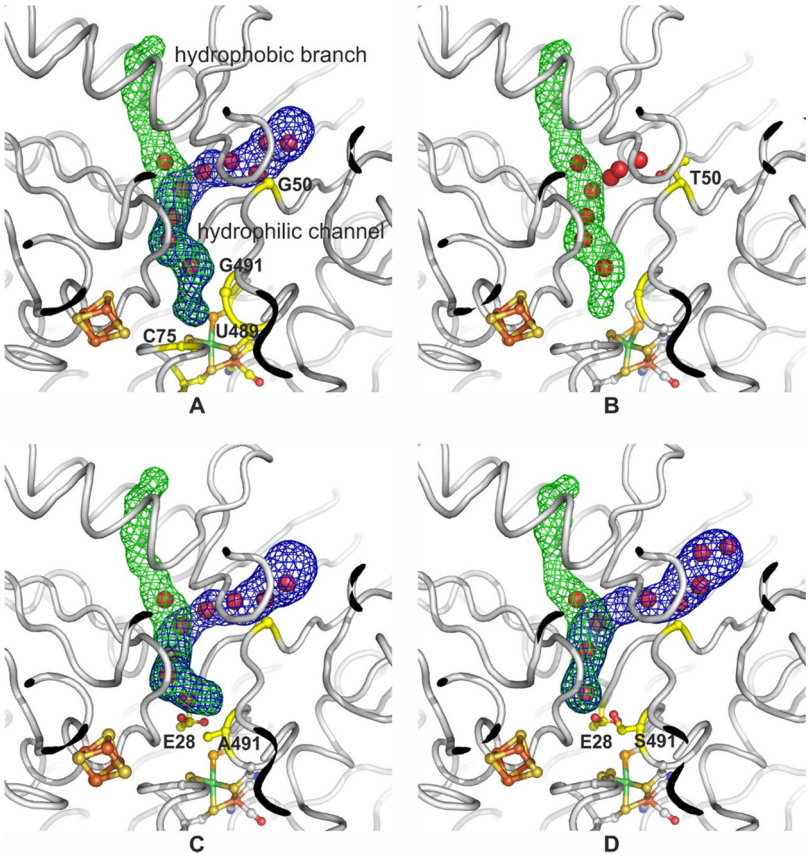

Figure 6. Close-up view of the channels in the structure of the *D. vulgaris* Hildenborough [NiFeSe] hydrogenase and variants, calculated with CAVER: (A) wild-type (PDB 5JSK); (B) G50T variant; (C) G491A variant; (D) G491S variant. The channels connecting the enzyme exterior with the Sec and the Cys75 Sγ atoms are displayed as meshes. The hydrophilic branch of the channel is shown in blue and the hydrophobic branch in green. The water molecules enclosed by the channels are represented as red spheres.

6 shows that the G50T mutation obstructs the hydrophilic branch (Figure 6B), while the G491A and G491S substitutions block channel access to Cys75 (Figure 6C,D).

DISCUSSION

In [NiFe] hydrogenases, the importance of hydrophobic gas channels was emphasized when experiments on O_2-tolerant regulatory hydrogenases (RH) revealed that bulky residues at the end of the hydrophobic channel narrow the access of gas molecules to the active site. This was initially proposed as the possible reason for the O_2 tolerance of these enzymes.[3,47,48] These observations prompted studies on the standard O_2-sensitive [NiFe] hydrogenase from *D. fructosovorans*, where bulky residues were introduced in the hydrophobic channel to restrict the access of inhibitory gases O_2 and CO. The effect of modifying the gas channel in the *D. fructosovorans* hydrogenase was to slow O_2 access to the active site[7] and also to increase the reactivation rates.[49] These mutations also resulted in strongly decreased H_2 production rates, since H_2 also diffuses through the same channel, in a step that limits the rate of H_2 production in these mutants.[49]

[NiFeSe] hydrogenases are powerful biocatalysts, which we aim to improve further by decreasing their O_2 sensitivity. Here, we tested mutations aiming to prevent the irreversible oxidation of Cys75. This residue is not directly accessible via the hydrophobic channel through which H_2 and O_2 are believed to diffuse; it is positioned at the end of a hydrophilic solvent channel that connects the active site of [NiFeSe] hydrogenases to the surface. This solvent channel seems to be present only in [NiFeSe] hydrogenases, since it is not seen in any of the O_2-resistant or O_2-sensitive [NiFe] hydrogenases that have been crystallized (Table S4). We tested the hypothesis that the hydrophilic channel leading to Cys75 also guides O_2 or ROS toward this residue, by examining how replacing amino acids whose side chains line this tunnel affects Cys75 oxidation and oxygen sensitivity. We observed that the G50T mutation has no significant effect, but both the G491A and G491S mutations significantly improve resistance against Cys75 irreversible oxidation. In protein film voltammetry experiments, the G491A and G491S variants are more slowly inactivated by O_2 than the WT, with 7-fold lower rate constants for O_2 inhibition. In addition, the results of solution assays show that the G491S variant is much more tolerant to prolonged air exposure, recovering nearly full activity even after overnight exposure to air. Therefore, our kinetic data reveal that the mutation prevents the formation of irreversibly oxidized species. From a molecular point of view, the X-ray structures of the variants show that the G491 mutations prevent the oxidation of Cys75. Channel prediction with CAVER explains why the G50T mutation has no effect on Cys75 oxidation: this residue is positioned at the entrance of the hydrophilic water channel, but a branching point in this channel still allows access of oxygen species to the active site in the G50T variant. In contrast, the G491 residue is close to the active site, and its substitution does prevent (or strongly delay) the access of oxidizing species to Cys75. In support of our

DOI: 10.1021/acscatal.9b02347
ACS Catal. 2019, 9, 8509−8519

hypothesis, we note that the oxidation of this terminal Ni ligand has never been observed in any [NiFe] hydrogenase where this tunnel is absent. Moreover, the rate of inhibition of the WT [NiFeSe] hydrogenase by O_2 (530 mM^{-1} s^{-1} at 40 °C) is well above the typical range observed with [NiFe] hydrogenases (5−20 mM^{-1} s^{-1}, from ref 42), whereas the G491 mutations decrease the rate of inhibition to a less remarkable value of around 80 mM^{-1} s^{-1}, which likely corresponds to O_2 diffusion through the hydrophobic channel as observed in standard [NiFe] hydrogenases.[42] This supports the idea that the mutations render ineffective the hydrophilic channel that is not present in [NiFe] hydrogenases.

Interestingly, the G491 mutations slow O_2 inhibition but have no effect on CO inhibition. Carbon monoxide is a competitive inhibitor of [NiFe] hydrogenases, and in the case of *D. fructosovorans* [NiFe] hydrogenase, the rate of inhibition by CO is limited by the rate of CO access to the active site.[5,7] Here we observed no correlation between changes in $k_{in}^{O_2}$ and k_{in}^{CO}, suggesting that, in *D. vulgaris* Hildenborough [NiFeSe] hydrogenase, the CO molecules diffuse preferentially through the hydrophobic channel system, whereas O_2/ROS diffuse more quickly through the hydrophilic channel system, as revealed by the inhibition kinetics.

Overall, our structural, biochemical, and electrochemical results provide strong support to the hypothesis that O_2 or ROS can reach the active site of *D. vulgaris* Hildenborough [NiFeSe] hydrogenase through a hydrophilic water channel. This argues against the general idea that aerobic inactivation occurs only through O_2 diffusion through hydrophobic channels. A few previous studies have also suggested that O_2 diffusion can occur through hydrophilic channels: in the enzyme nitrogenase it has been observed that a hydrophilic channel is used for transport of the nonpolar substrate N_2.[50,51] In catalase, MD simulations indicate that the same channel is used by substrates and products, H_2O_2, H_2O, and O_2.[52] Interestingly, in O_2-tolerant hydrogenases it has been proposed that hydrophilic channels are involved in removal of the water molecules produced during H_2 oxidation in the presence of O_2.[53]

All *D. vulgaris* [NiFeSe] hydrogenase variants studied here are slightly less active than the WT but still more active than any [NiFe] hydrogenase. Residue 491 is close to the highly conserved Glu28 (Figure 6C,D), which in [NiFe] hydrogenases is part of the proton transfer pathway.[54] A plausible explanation for the mutation-induced decrease in activity is that the bulkier side chains of the G491 variants may place some steric hindrance in the side-chain motion of Glu28 and thus interfere with proton transfer. This could be especially relevant in the case of the G491S variant, where in the crystal structure Ser491 forms a hydrogen bond with Glu28 that could further hinder the proton transfer action of Glu28. Indeed, as shown in Table 1, the H_2 evolution activities of the variants are more affected than those of H_2 oxidation, and particularly so in the case of G491S. In the G50T variant, the threonine side chain breaks the chain of water molecules in the hydrophilic channel, possibly creating a barrier to proton transfer and thus lowering the enzyme activity. Proton transfer is proposed to be the rate-limiting step of H_2 production in the WT form of *D. fructosovorans* [NiFe] hydrogenase.[55] If proton transfer also limits the rate of H_2 production by *D. vulgaris* Hildenborough [NiFeSe] hydrogenase, then mutations that interfere with the proton transfer pathway should slow H_2 evolution more than H_2 uptake, as indeed observed in our experiments (Table 1).

The oxidation of Cys75 to the sulfinate state is also expected to lower the activity of the G491S variant. This modification is apparently formed during prolonged air exposure (long purification and crystallization), since we observe reduced levels of Cys75 sulfinate in aerobically crystallized samples after starting to work with recombinant protein (~60% vs 100% previously), for which affinity purification is much faster.[18] We have previously measured the decrease in activity of the WT enzyme under the crystallization conditions[56] and observed a gradual loss of activity, reaching about 10% after 10 days. This indicates that formation of Cys75 sulfinate leads to activity reduction, but whether the modified form retains any activity or not is difficult to ascertain. The observation that the reduced form (conformer III) could still be obtained by H_2 reduction of aerobic crystals,[27] where Cys75 sulfinate was already present in most molecules, may suggest that some activity is retained. On the other hand, the precision of the crystallographic assignments for the sulfinate state is about ±10%; thus, we cannot discard that there were some active enzyme molecules left without the sulfinate modification, which were sufficient to generate enough electrons inside the crystal leading to reduction of the sulfinate-modified molecules (also obtained with dithionite[27]).

CONCLUDING REMARKS

In conclusion, we show that a single mutation (G491A or G491S) can improve the O_2 tolerance of a [NiFeSe] hydrogenase, while it retains high activity in both directions of H_2 catalysis. Both variants exhibit a lower rate of inactivation by O_2 and a faster rate of reactivation after O_2 exposure. These results emphasize the fact that the O_2 sensitivity of hydrogenases from different families may be determined by specific structural features. Furthermore, our results also reveal that O_2 and/or ROS can access the active site of [NiFeSe] hydrogenase through a hydrophilic channel, in contrast with the general assumption that O_2 molecules are guided only by hydrophobic channels.

METHODS

Variant Expression and Purification. The *D. vulgaris* Hildenborough [NiFeSe] hydrogenase variants were created by site-directed mutagenesis with an NZYMutagenesis kit (Nzytech) using the expression vector pMOIP03 carrying a *hys*A_{Strep}*hys*B fragment as a template.[18,31] The vectors were electroporated into the IPAR01 deletion strain,[18] using the Gene Pulser XCell apparatus (Biorad) at 1250 V, 250 Ω, and 25 μF.[57] Cells were grown at 37 °C in standard lactate−sulfate medium supplement with 1 μM $NiCl_2{\cdot}6H_2O$ and 1 μM $NaSeO_3{\cdot}5H_2O$. Cells were collected and disrupted in the French press at 6.9 MPa. The expression of the protein variants was assessed by Western blot against native *D. vulgaris* Hildenborough [NiFeSe] hydrogenase and against the Strep-Tactin AP (IBA Lifesciences). For purification the soluble fraction was first applied in a Q-Sepharose HP column (XK 26/10, GE Healthcare) equilibrated with 20 mM Tris-HCl pH 7.6 and a stepwise NaCl gradient of 50 mM/step was performed. Fractions with [NiFeSe] hydrogenase activity were affinity-purified using a gravity column containing Strep-Tactin resin (IBA Lifesciences) equilibrated with 100 mM Tris-HCl pH 8.0 and 150 mM NaCl (buffer W); the recombinant protein was eluted with buffer W plus 2.5 mM desthiobiotin.

DOI: 10.1021/acscatal.9b02347
ACS Catal. 2019, 9, 8509−8519

The purity of [NiFeSe] hydrogenase WT and variants was analyzed by SDS-PAGE stained with Comassie Blue.

Hydrogenase Activities. H_2-oxidation activity was routinely determined spectrophotometrically by following the H_2-dependent reduction of methylviologen (MV) at 604 nm (ε = 13.6 mM^{-1} cm^{-1}) at 30 °C inside a Coy anaerobic chamber (98% N_2, 2% H_2). The assay solution contained 2 mM MV in H_2-saturated 50 mM Tris-HCl buffer at pH 8, and the as-isolated enzyme was previously activated with 0.5 bar H_2 for 30 min. One unit of enzyme is defined as the amount of hydrogenase reducing 2 μmol of MV per minute, which is equivalent to 1 μmol of H_2 oxidized per minute.

For H_2 production the enzyme was reduced with 1 mM methylviologen (MV) reduced by 15 mM sodium dithionite and the reaction mixture was incubated in a shaker at 37 °C for 10 min. A headspace sample was measured, every 4 min, in a Trace GC Ultra gas chromatograph (Thermo Scientific) equipped with a thermal conductivity detector and a MolSieve 5A 80/100 column (Althech) with N_2 as a carrier gas.

Electrochemistry. All electrochemical experiments were carried out in a glovebox (Jacomex) filled with N_2, with the electrochemical setup and equipment as previously described.[40] We used a pyrolytic graphite edge (PGE) rotating disk working electrode (area ~3 mm^2), a platinum wire as a counter electrode, and a saturated calomel electrode (SCE), located in a Luggin side arm of the electrochemical cell and immersed in 0.1 M NaCl, as a reference. The enzyme was coadsorbed with neomycin[58] on the working electrode. The electrode surface was first polished with an aqueous alumina slurry (1 μm) and sonicated. Then it was covered with 0.5 μL of neomycin (200 mg/mL in water) and 1 μL of the *D. vulgaris* Hildenborough [NiFeSe] hydrogenase (50 μg/mL in pH 7 mixed buffer consisting of 5 mM MES, 5 mM CHES, 5 mM HEPES, 5 mM TAPS, 5 mM sodium acetate, and 100 mM NaCl). The protein film was allowed to dry and then rinsed with water. The electrochemical cell contained pH 7 mixed buffer and was continuously flushed with pure H_2. The temperature was regulated at 40 °C by circulating water in the double jacket of the cell. The data were analyzed using QSoas,[59] an open source program available at http://www.qsoas.org.

O_2 Tolerance Studies in Solution. Samples of the as-isolated enzymes (0.25 μM) were activated for 1 h in 0.5 bar H_2, 50 mM Tris-HCl pH 8, and 1 mM MV and were kept under an H_2 atmosphere overnight. The H_2 oxidation activity was measured and taken as corresponding to the maximum activity of each protein. Next, the enzyme solutions were put in contact with air and diluted to 0.125 μM in an aerobic buffer of 50 mM Tris-HCl pH 8. Three samples of each enzyme solution were kept under aerobic conditions for 1 h, 4 h, or overnight (~16 h) at room temperature, after which no H_2 oxidation activity was detected in any of the samples. Following this air exposure, oxidized MV was added to each sample up to a concentration of 1 mM, and the enzymes were reactivated again under 0.5 bar H_2 for 10, 30, or 90 min, following which H_2 oxidation activities were measured.

Crystallization and X-ray Diffraction Data Collection. Crystals of the three *D. vulgaris* [NiFeSe] hydrogenase variants were obtained at 20 °C by the sitting drop variant of the vapor diffusion method. Drops of 1 or 2 μL of pure protein (80−114 μM) were mixed with an equal volume of reservoir solution containing 20% PEG 1500 (w/v) and 100 mM Tris-HCl pH 7 and equilibrated against 500 μL of the reservoir solution.

Crystals appeared after about 1 week and were harvested, briefly dipped in a cryoprotecting solution with the same composition as the reservoir solution and adjusted to include 10% (v/v) glycerol, flash-cooled in liquid nitrogen, and shipped to a synchrotron beamline for data collection. The G50T and G491S data sets were collected at the European Synchrotron Radiation Facility (ESRF, Grenoble, France) at beamlines ID29 and ID30A-3, respectively, and the G491A data set was measured at the beamline I03 of the Diamond Light Source (DLS, Didcot, U.K.). The data collection and processing statistics are given in Table S1.

The G50T and G491A data sets were integrated with XDS[60] and AutoPROC,[61] analyzed with POINTLESS,[62] and scaled and merged with STARANISO[63] and AIMLESS.[64] The G491A data set was integrated and scaled with XDS, analyzed with POINTLESS, and merged with AIMLESS.

Structure Determination and Refinement. The crystal structures were determined by the molecular replacement method with PHASER[65] via the CCP4 Graphics User Interface.[66] The coordinates of the protein chains of the large and small subunits of the previously published crystal structure of *D. vulgaris* [NiFeSe] hydrogenase (PDB 5JSH)[18] were used as search models, after removal of all nonprotein atoms. Following a quick initial refinement with REFMAC,[67] COOT[68] was used to perform model corrections and addition of the active site metals and Fe−S clusters. Refinement was continued with PHENIX,[45] consisting of five macrocycles with refinement of positional coordinates, individual isotropic atomic displacement parameters for all non-hydrogen atoms, and anomalous dispersion parameters for the Se atom. Model inspection and editing was done with COOT against σ_A-weighted $2|F_o| - |F_c|$ and $|F_o| - |F_c|$ electron density maps. Water molecules were added with PHENIX and checked with COOT. Hydrogen atoms in calculated positions were added to the structural models and included in the refinement in riding positions. In the final refinement stages, individual anisotropic atomic displacement parameters for all protein non-hydrogen atoms were refined for structures G50T and G491S. For structure G491A, TLS (translation-libration-screw) rigid body refinement of atomic displacement parameters was carried out instead, followed by refinement of individual isotropic *B* factors. Six and seven TLS groups were used respectively for the small subunit (chain A) and the large subunit (chain B). These groups were adapted from the list determined with the *find_tls_groups* tool in PHENIX from a previous full isotropic refinement to also include the active site and the iron−sulfur clusters.

MOLPROBITY[69] was used to investigate the model geometry in combination with the validation tools provided in COOT: for all three crystal structures reported here, the number of Ramachandran outliers did not exceed 0.13% of the total number of nonproline and nonglycine residues and the clash score did not exceed 2.5. The refinement statistics are included in Table S2.

Structure figures were created using the PyMOL Molecular Graphics System, Version 2.1.0 Open Source (Schrödinger, LLC). CAVER calculations were done using the PyMOL plug-in with default parameters (minimum probe radius of 0.9 Å, shell depth of 4 Å, shell radius of 3 Å, a clustering threshold of 3.5, and a starting point optimization with 3 Å maximum distance and a desired radius of 5 Å) and atomic coordinates including hydrogen atoms in calculated positions. The final atomic coordinates and experimental structure factors were

DOI: 10.1021/acscatal.9b02347
ACS Catal. 2019, 9, 8509−8519

deposited in the Worldwide Protein Data Bank[70] with accession codes 6RTP, 6RU9, and 6RUC for the G50T, G491A, and G491S structures, respectively.

■ ASSOCIATED CONTENT

Supporting Information

The Supporting Information is available free of charge on the ACS Publications website at DOI: 10.1021/acscatal.9b02347.

View of the active site conformations in the as-isolated *D. vulgaris* Hildenborough [NiFeSe] hydrogenase, structure-based sequence alignments used to select the *D. vulgaris* Hildenborough [NiFeSe] hydrogenase mutants, X-ray data collection, processing, and refinement statistics, structural details at the active site and proximal [Fe_4S_4] cluster, views of the active site of the aerobically purified and crystallized [NiFeSe] hydrogenase G50T and G491S variants, H_2 uptake activity of WT and variants, channels predicted by CAVER in [NiFe] and [NiFeSe] hydrogenase structures, detailed views of the hydrophilic channel and hydrophobic side channel, and graph showing the effect of CO on the H_2 oxidation current of WT [NiFeSe] hydrogenase and variants adsorbed onto a graphite rotating electrode (PDF)

■ AUTHOR INFORMATION

Corresponding Authors

*E-mail for P.M.M.: matias@itqb.unl.pt.
*E-mail for I.A.C.P.: ipereira@itqb.unl.pt.

ORCID

Melisa del Barrio: 0000-0002-6947-6686
Vincent Fourmond: 0000-0001-9837-6214
Christophe Léger: 0000-0002-8871-6059
Pedro M. Matias: 0000-0001-6170-451X

Notes

The authors declare no competing financial interest.

■ ACKNOWLEDGMENTS

This work was financially supported by Fundação para a Ciência e Tecnologia (Portugal) through fellowship SFRH/BD/100314/2014 (to S.Z.), grant PTDC/BBB-BEP/2885/2014 (to P.M.M. and I.A.C.P.), and R&D units UID/Multi/04551/2013 (Green-IT) and LISBOA-01-0145-FEDER-007660 (MostMicro) cofunded by FCT/MCTES and FEDER funds through COMPETE2020/POCI. The work of M. del B., V. F., and C. L. was supported by CNRS, Aix Marseille Université, Agence Nationale de la Recherche (ANR-14-CE05-0010), and the Excellence Initiative of AixMarseille University - A*MIDEX, a French "Investissements d'Avenir" programme (ANR-11-IDEX-0001-02). Support from the ESRF and the beamline staff of ID29 and ID30A-3 for the G50T and G491S data collections is acknowledged, and we also thank Diamond Light Source for access to beamline I02 under proposal number MX10515 for the G491A data collection. Funding from the European Union's Horizon 2020 research and innovation programme under grant agreement No. 810856 is also acknowledged, and the French authors are part of the French bioinorganic chemistry research network (www.frenchbic.cnrs.fr).

■ REFERENCES

(1) Lubitz, W.; Ogata, H.; Rudiger, O.; Reijerse, E. Hydrogenases. *Chem. Rev.* **2014**, *114*, 4081−4148.
(2) Montet, Y.; Amara, P.; Vernede, X.; Hatchikian, E. C.; Field, M.; Frey, M.; Fontecilla-Camps, J. C. Gas Access to the Active Site of Ni-Fe Hydrogenases Probed by X-Ray Crystallography and Molecular Dynamics. *Nat. Struct. Biol.* **1997**, *4*, 523−526.
(3) Volbeda, A.; Montet, Y.; Vernâ, X.; Hatchikian, E. C.; Fontecilla-camps, J. C. High-Resolution Crystallographic Analysis of *Desulfovibrio Fructosovorans* [NiFe] Hydrogenase. *Int. J. Hydrogen Energy* **2002**, *27*, 1449−1461.
(4) Teixeira, V.; Baptista, A.; Soares, C. M. Pathways of H_2 toward the Active Site of [NiFe]-Hydrogenase. *Biophys. J.* **2006**, *91*, 2035−2045.
(5) Leroux, F.; Dementin, S.; Burlat, B.; Cournac, L.; Volbeda, A.; Champ, S.; Martin, L.; Guigliarelli, B.; Bertrand, P.; Fontecilla-Camps, J. C.; Rousset, M.; Léger, C. Experimental Approaches to Kinetics of Gas Diffusion in Hydrogenase. *Proc. Natl. Acad. Sci. U. S. A.* **2008**, *105*, 11188−11193.
(6) Fontecilla-Camps, J. C.; Amara, P.; Cavazza, C.; Nicolet, Y.; Volbeda, A. Structure-Function Relationships of Anaerobic Gas-Processing Metalloenzymes. *Nature* **2009**, *460*, 814−822.
(7) Liebgott, P.; Leroux, F.; Burlat, B.; Dementin, S.; Baffert, C.; Lautier, T.; Fourmond, V.; Ceccaldi, P.; Cavazza, C.; Meynial-Salles, I.; Soucaille, P.; Fontecilla-Camps, J. C.; Guigliarelli, B.; Bertrand, P.; Rousset, M.; Léger, C. Relating Diffusion along the Substrate Tunnel and Oxygen Sensitivity in Hydrogenase. *Nat. Chem. Biol.* **2010**, *6*, 63−70.
(8) Kalms, J.; Schmidt, A.; Frielingsdorf, S.; Van Der Linden, P.; Von Stetten, D.; Lenz, O.; Carpentier, P.; Scheerer, P. Krypton Derivatization of an O_2-Tolerant Membrane-Bound [NiFe] Hydrogenase Reveals a Hydrophobic Tunnel Network for Gas Transport. *Angew. Chem., Int. Ed.* **2016**, *55*, 5586−5590.
(9) Kalms, J.; Schmidt, A.; Frielingsdorf, S.; Utesch, T.; Gotthard, G.; von Stetten, D.; van der Linden, P.; Royant, A.; Mroginski, M. A.; Carpentier, P.; Lenz, O.; Scheerer, P. Tracking the Route of Molecular Oxygen in O_2-Tolerant Membrane-Bound [NiFe] Hydrogenase. *Proc. Natl. Acad. Sci. U. S. A.* **2018**, *115* (10), E2229−E2237.
(10) Kubas, A.; Orain, C.; De Sancho, D.; Saujet, L.; Sensi, M.; Gauquelin, C.; Meynial-Salles, I.; Soucaille, P.; Bottin, H.; Baffert, C.; Fourmond, V.; Best, R.; Blumberger, J.; Léger, C. Mechanism of O_2 Diffusion and Reduction in FeFe Hydrogenases. *Nat. Chem.* **2017**, *9*, 88−95.
(11) Fernández, V. M.; Hatchikian, E. C.; Cammack, R. Properties and Reactivation of Two Different Deactivated Forms of *Desulfovibrio Gigas* Hydrogenase. *Biochim. Biophys. Acta, Protein Struct. Mol. Enzymol.* **1985**, *832*, 69−79.
(12) Lamle, S. E.; Albracht, S. P. J.; Armstrong, F. A. Electrochemical Potential-Step Investigations of the Aerobic Interconversions of [NiFe]-Hydrogenase from *Allochromatium Vinosum*: Insights into the Puzzling Difference between Unready and Ready Oxidized Inactive States. *J. Am. Chem. Soc.* **2004**, *126*, 14899−14909.
(13) Abou Hamdan, A.; Burlat, B.; Gutiérrez-Sanz, Ó.; Liebgott, P.; Baffert, C.; De Lacey, A. L.; Rousset, M.; Guigliarelli, B.; Léger, C.; Dementin, S. O_2-Independent Formation of the Inactive States of NiFe Hydrogenase. *Nat. Chem. Biol.* **2013**, *9*, 15−17.
(14) Baltazar, C.; Marques, M.; Soares, C. M.; De Lacey, A.; Pereira, I. A. C.; Matias, P. M. Nickel-Iron-Selenium Hydrogenases - An Overview. *Eur. J. Inorg. Chem.* **2011**, *2011*, 948−962.
(15) Wombwell, C.; Caputo, C. A.; Reisner, E. [NiFeSe]-Hydrogenase Chemistry. *Acc. Chem. Res.* **2015**, *48*, 2858−2865.
(16) Teixeira, M.; Fauque, G.; Moura, I.; Lespinat, P. A.; Berlier, Y.; Prickril, B.; Peck, H.; Xavier, A. V.; Gall, J. Le; Moura, J. J. G. Nickel-[Iron-Sulfur]-Selenium-Containing Hydrogenases from *Desulfovibrio Baculatus* (DSM 1743). *Eur. J. Biochem.* **1987**, *167*, 47−58.
(17) Valente, F.; Oliveira, S.; Gnadt, N.; Pacheco, I.; Coelho, A. V.; Xavier, A. V.; Teixeira, M.; Soares, C. M.; Pereira, I. A. C. Hydrogenases in *Desulfovibrio Vulgaris* Hildenborough: Structural

DOI: 10.1021/acscatal.9b02347
ACS Catal. 2019, 9, 8509−8519

and Physiologic Characterisation of the Membrane-Bound [NiFeSe] Hydrogenase. *JBIC, J. Biol. Inorg. Chem.* **2005**, *10*, 667−682.
(18) Marques, M.; Tapia, C.; Gutiérrez-Sanz, Ó.; Ramos, A. R.; Keller, K. L.; Wall, J. D.; De Lacey, A. L.; Matias, P. M.; Pereira, I. A. C. The Direct Role of Selenocysteine in [NiFeSe] Hydrogenase Maturation and Catalysis. *Nat. Chem. Biol.* **2017**, *13*, 544−550.
(19) Parkin, A.; Goldet, G.; Cavazza, C.; Fontecilla-Camps, J. C.; Armstrong, F. A. The Difference a Se Makes? Oxygen-Tolerant Hydrogen Production by the [NiFeSe]-Hydrogenase from *Desulfomicrobium Baculatum*. *J. Am. Chem. Soc.* **2008**, *130*, 13410−13416.
(20) Reisner, E.; Powell, D. J.; Cavazza, C.; Fontecilla-Camps, J. C.; Armstrong, F. A. Visible Light-Driven H_2 Production by Hydrogenases Attached to Dye-Sensitized TiO_2 Nanoparticles. *J. Am. Chem. Soc.* **2009**, *131*, 18457−18466.
(21) Wakerley, D. W.; Reisner, E. Oxygen-Tolerant Proton Reduction Catalysis: Much O2 about Nothing? *Energy Environ. Sci.* **2015**, *8*, 2283−2295.
(22) Baltazar, C.; Teixeira, V. H.; Soares, C. M. Structural Features of [NiFeSe] and [NiFe] Hydrogenases Determining Their Different Properties: A Computational Approach. *JBIC, J. Biol. Inorg. Chem.* **2012**, *17*, 543−555.
(23) Gutiérrez-Sanz, Ó.; Marques, M.; Baltazar, C.; Fernández, V. M.; Soares, C. M.; Pereira, I. A. C.; De Lacey, A. L. Influence of the Protein Structure Surrounding the Active Site on the Catalytic Activity of [NiFeSe] Hydrogenases. *JBIC, J. Biol. Inorg. Chem.* **2013**, *18*, 419−427.
(24) Tamura, T.; Tsunekawa, N.; Nemoto, M.; Inagaki, K.; Hirano, T.; Sato, F. Molecular Evolution of Gas Cavity in [NiFeSe] Hydrogenases Resurrected *in Silico*. *Sci. Rep.* **2016**, *6*, 19742.
(25) Ceccaldi, P.; Marques, M.; Fourmond, V.; Pereira, I. A. C.; Léger, C. Oxidative Inactivation of NiFeSe Hydrogenase. *Chem. Commun.* **2015**, *51*, 14223−14226.
(26) Maroney, M. J.; Hondal, R. J. Selenium versus Sulfur: Reversibility of Chemical Reactions and Resistance to Permanent Oxidation in Proteins and Nucleic Acids. *Free Radical Biol. Med.* **2018**, *127*, 228−237.
(27) Marques, M.; Coelho, R.; Pereira, I. A. C.; Matias, P. M. Redox State-Dependent Changes in the Crystal Structure of [NiFeSe] Hydrogenase from Desulfovibrio Vulgaris Hildenborough. *Int. J. Hydrogen Energy* **2013**, *38*, 8664−8682.
(28) Marques, M.; Coelho, R.; De Lacey, A. L.; Pereira, I. A. C.; Matias, P. M. The Three-Dimensional Structure of [NiFeSe] Hydrogenase from *Desulfovibrio Vulgaris* Hildenborough: A Hydrogenase without a Bridging Ligand in the Active Site in Its Oxidised, "as-Isolated" State. *J. Mol. Biol.* **2010**, *396*, 893−907.
(29) Volbeda, A.; Amara, P.; Iannello, M.; De Lacey, A. L.; Cavazza, C.; Fontecilla-Camps, J. C. Structural Foundations for the O_2 Resistance of *Desulfomicrobium Baculatum* [NiFeSe]-Hydrogenase. *Chem. Commun. (Cambridge, U. K.)* **2013**, *49*, 7061−7063.
(30) Garcin, E.; Vernede, X.; Hatchikian, E. C.; Volbeda, A.; Frey, M.; Fontecilla-Camps, J. C. The Crystal Structure of a Reduced [NiFeSe] Hydrogenase Provides an Image of the Activated Catalytic Center. *Structure* **1999**, *7*, 557−566.
(31) Zacarias, S.; Vélez, M.; Pita, M.; De Lacey, A. L.; Matias, P. M.; Pereira, I. A. C. *Methods in Enzymology* **2018**, *613*, 169.
(32) Ruff, A.; Szczesny, J.; Zacarias, S.; Pereira, I. A. C.; Plumeré, N.; Schuhmann, W. Protection and Reactivation of the [NiFeSe] Hydrogenase from *Desulfovibrio Vulgaris* Hildenborough under Oxidative Conditions. *ACS Energy Lett.* **2017**, *2*, 964−968.
(33) Ruff, A.; Szczesny, J.; Marković, N.; Conzuelo, F.; Zacarias, S.; Pereira, I. A. C.; Lubitz, W.; Schuhmann, W. A Fully Protected Hydrogenase/Polymer-Based Bioanode for High-Performance Hydrogen/Glucose Biofuel Cells. *Nat. Commun.* **2018**, *9*, 3675.
(34) Szczesny, J.; Marković, N.; Conzuelo, F.; Zacarias, S.; Pereira, I. A. C.; Lubitz, W.; Plumeré, N.; Schuhmann, W.; Ruff, A. A Gas Breathing Hydrogen/Air Biofuel Cell Comprising a Redox Polymer/Hydrogenase-Based Bioanode. *Nat. Commun.* **2018**, *9*, 4715.
(35) Tapia, C.; Zacarias, S.; Pereira, I. A. C.; Conesa, J. C.; Pita, M.; De Lacey, A. L. *In Situ* Determination of Photobioproduction of H_2 by In_2S_3-[NiFeSe] Hydrogenase from *Desulfovibrio Vulgaris* Hildenborough Using Only Visible Light. *ACS Catal.* **2016**, *6*, 5691−5698.
(36) Gutiérrez-Sanz, Ó.; Natale, P.; Márquez, I.; Marques, M.; Zacarias, S.; Pita, M.; Pereira, I. A. C.; López-Montero, I.; De Lacey, A. L.; Vélez, M. H_2-Fueled ATP Synthesis on an Electrode: Mimicking Cellular Respiration. *Angew. Chem., Int. Ed.* **2016**, *55*, 6216−6220.
(37) Paulsen, C. E.; Carroll, K. S. Cysteine-Mediated Redox Signaling: Chemistry, Biology, and Tools for Discovery. *Chem. Rev.* **2013**, *113*, 4633−4679.
(38) Sensi, M.; del Barrio, M.; Baffert, C.; Fourmond, V.; Léger, C. New Perspectives in Hydrogenase Direct Electrochemistry. *Curr. Opin. Electrochem.* **2017**, *5*, 135−145.
(39) del Barrio, M.; Sensi, M.; Orain, C.; Baffert, C.; Dementin, S.; Fourmond, V.; Léger, C. Electrochemical Investigations of Hydrogenases and Other Enzymes That Produce and Use Solar Fuels. *Acc. Chem. Res.* **2018**, *51*, 769−777.
(40) Léger, C.; Dementin, S.; Bertrand, P.; Rousset, M.; Guigliarelli, B. Inhibition and Aerobic Inactivation Kinetics of *Desulfovibrio Fructosovorans* NiFe Hydrogenase Studied by Protein Film Voltammetry. *J. Am. Chem. Soc.* **2004**, *126*, 12162−12172.
(41) Fourmond, V.; Lautier, T.; Baffert, C.; Leroux, F.; Liebgott, P.; Dementin, S.; Rousset, M.; Arnoux, P.; Pignol, D.; Meynial-Salles, I.; Soucaille, P.; Bertrand, P.; Léger, C. Correcting for Electrocatalyst Desorption and Inactivation in Chronoamperometry Experiments. *Anal. Chem.* **2009**, *81*, 2962.
(42) del Barrio, M.; Guendon, C.; Kpebe, A.; Baffert, C.; Fourmond, V.; Brugna, M.; Léger, C. A Valine-to-Cysteine Mutation Further Increases the Oxygen Tolerance of *Escherichia Coli* NiFe Hydrogenase Hyd-1. *ACS Catal.* **2019**, *9*, 4084−4088.
(43) Almeida, M. G.; Silveira, C. M.; Guigliarelli, B.; Bertrand, P.; Moura, J. J. G.; Moura, I.; Léger, C. A Needle in a Haystack: The Active Site of the Membrane-Bound Complex Cytochrome *c* Nitrite Reductase. *FEBS Lett.* **2007**, *581*, 284−288.
(44) Chovancova, E.; Pavelka, A.; Benes, P.; Strnad, O.; Brezovsky, J.; Kozlikova, B.; Gora, A.; Sustr, V.; Klvana, M.; Medek, P.; Biedermannova, L.; Sochor, J.; Damborsky, J. CAVER 3.0: A Tool for the Analysis of Transport Pathways in Dynamic Protein Structures. *PLoS Comput. Biol.* **2012**, *8*, No. e1002708.
(45) Adams, P. D.; Afonine, P. V.; Bunkóczi, G.; Chen, V. B.; Davis, I. W.; Echols, N.; Headd, J. J.; Hung, L. W.; Kapral, G. J.; Grosse-Kunstleve, R. W.; McCoy, A.; Moriarty, N.; Oeffner, R.; Read, R.; Richardson, D.; Richardson, J.; Terwilliger, T.; Zwart, P. PHENIX: A Comprehensive Python-Based System for Macromolecular Structure Solution. *Acta Crystallogr., Sect. D: Biol. Crystallogr.* **2010**, *66*, 213−221.
(46) Ogata, H.; Nishikawa, K.; Lubitz, W. Hydrogens Detected by Subatomic Resolution Protein Crystallography in a [NiFe] Hydrogenase. *Nature* **2015**, *520*, 571−574.
(47) Buhrke, T.; Lenz, O.; Krauss, N.; Friedrich, B. Oxygen Tolerance of the H_2-Sensing [NiFe] Hydrogenase from *Ralstonia Eutropha* H16 Is Based on Limited Access of Oxygen to the Active Site. *J. Biol. Chem.* **2005**, *280*, 23791−23796.
(48) Duché, O.; Elsen, S.; Cournac, L.; Colbeau, A. Enlarging the Gas Access Channel to the Active Site Renders the Regulatory Hydrogenase HupUV of *Rhodobacter Capsulatus* O_2 Sensitive without Affecting Its Transductory Activity. *FEBS J.* **2005**, *272*, 3899−3908.
(49) Abou Hamdan, A.; Liebgott, P.; Fourmond, V.; Gutiérrez-Sanz, Ó.; De Lacey, A. L.; Infossi, P.; Rousset, M.; Dementin, S.; Léger, C. Relation between Anaerobic Inactivation and Oxygen Tolerance in a Large Series of NiFe Hydrogenase Mutants. *Proc. Natl. Acad. Sci. U. S. A.* **2012**, *109*, 19916−19921.
(50) Durrant, M. C. Controlled Protonation of Iron−Molybdenum Cofactor by Nitrogenase: A Structural and Theoretical Analysis. *Biochem. J.* **2001**, *355*, 569−576.
(51) Barney, B. M.; Yurth, M. G.; Santos, P. C.; Dean, D. R.; Seefeldt, C.; Carolina, N. A Substrate Channel in the Nitrogenase MoFe Protein. *JBIC, J. Biol. Inorg. Chem.* **2009**, *14*, 1015−1022.

DOI: 10.1021/acscatal.9b02347
ACS Catal. 2019, 9, 8509−8519

(52) Amara, P.; Andreoletti, P.; Jouve, H. M.; Field, M. J. Ligand Diffusion in the Catalase from Proteus Mirabilis: A Molecular Dynamics Study. *Protein Sci.* **2001**, *10*, 1927−1935.
(53) Fritsch, J.; Scheerer, P.; Frielingsdorf, S.; Kroschinsky, S.; Friedrich, B.; Lenz, O.; Spahn, C. M. T. The Crystal Structure of an Oxygen-Tolerant Hydrogenase Uncovers a Novel Iron-Sulphur Centre. *Nature* **2011**, *479*, 249−252.
(54) Dementin, S.; Burlat, B.; De Lacey, A. L.; Pardo, A.; Adryanczyk-Perrier, G.; Guigliarelli, B.; Fernández, V. M.; Rousset, M. A Glutamate Is the Essential Proton Transfer Gate during the Catalytic Cycle of the [NiFe] Hydrogenase. *J. Biol. Chem.* **2004**, *279*, 10508−10513.
(55) Bertrand, P.; Dole, F.; Asso, M.; Guigliarelli, B. Is There a Rate-Limiting Step in the Catalytic Cycle of [Ni-Fe] Hydrogenases? *JBIC, J. Biol. Inorg. Chem.* **2000**, *5*, 682−691.
(56) Marques, M. F. C. Ph.D. Thesis, *Structural and Functional Studies of a High Activity NiFeSe Hydrogenase*; Universidade Nova de Lisboa: Oeiras, 2014.
(57) Keller, K. L.; Wall, J. D.; Chhabra, S.; Voigt, C. *Methods Enzymol.* **2011**, *497*, 503.
(58) Bertrand, P.; Frangioni, B.; Dementin, S.; Sabaty, M.; Arnoux, P.; Guigliarelli, B.; Pignol, D.; Léger, C. Effects of Slow Substrate Binding and Release in Redox Enzymes: Theory and Application to Periplasmic Nitrate Reductase. *J. Phys. Chem. B* **2007**, *111*, 10300−10311.
(59) Fourmond, V. QSoas: A Versatile Software for Data Analysis. *Anal. Chem.* **2016**, *88*, 5050−5052.
(60) Kabsch, W. XDS. *Acta Crystallogr., Sect. D: Biol. Crystallogr.* **2010**, *66*, 125−132.
(61) Vonrhein, C.; Flensburg, C.; Keller, P.; Sharff, A.; Smart, O.; Paciorek, W.; Womack, T.; Bricogne, G. Data Processing and Analysis with the AutoPROC Toolbox. *Acta Crystallogr., Sect. D: Biol. Crystallogr.* **2011**, *67*, 293−302.
(62) Evans, P. Scaling and Assessment of Data Quality. *Acta Crystallogr., Sect. D: Biol. Crystallogr.* **2006**, *62*, 72−82.
(63) Tickle, I. J.; Flensburg, C.; Keller, P.; Paciorek, W.; Sharff, A.; Vonrhein, C.; Bricogne, G. *STARANISO*; Global Phasing: Cambridge, United Kingdom, 2018.
(64) Evans, P. R.; Murshudov, G. N. How Good Are My Data and What Is the Resolution? *Acta Crystallogr., Sect. D: Biol. Crystallogr.* **2013**, *69*, 1204−1214.
(65) McCoy, A. J. Solving Structures of Protein Complexes by Molecular Replacement with Phaser. *Acta Crystallogr., Sect. D: Biol. Crystallogr.* **2007**, *63*, 32−41.
(66) Potterton, E.; Briggs, P.; Turkenburg, M.; Dodson, E. A Graphical User Interface to the CCP4 Program Suite Research Papers A Graphical User Interface to the CCP 4 Program Suite. *Acta Crystallogr., Sect. D: Biol. Crystallogr.* **2003**, *59*, 1131−1137.
(67) Murshudov, G. N.; Skubák, P.; Lebedev, A. A.; Pannu, N. S.; Steiner, R. A.; Nicholls, R. A.; Winn, M. D.; Long, F.; Vagin, A. A. REFMAC5 for the Refinement of Macromolecular Crystal Structures. *Acta Crystallogr., Sect. D: Biol. Crystallogr.* **2011**, *67*, 355−367.
(68) Emsley, P.; Lohkamp, B.; Scott, W. G.; Cowtan, K. Features and Development of Coot. *Acta Crystallogr., Sect. D: Biol. Crystallogr.* **2010**, *66*, 486−501.
(69) Chen, V. B.; Arendall, W. B.; Headd, J. J.; Keedy, D. A.; Immormino, R. M.; Kapral, G. J.; Murray, L. W.; Richardson, J. S.; Richardson, D. C.; Richardson, D. C. MolProbity: All-Atom Structure Validation for Macromolecular Crystallography. *Acta Crystallogr., Sect. D: Biol. Crystallogr.* **2010**, *66*, 12−21.
(70) Berman, H.; Henrick, K.; Nakamura, H. Announcing the Worldwide Protein Data Bank. *Nat. Struct. Mol. Biol.* **2003**, *10*, 980−980.

DOI: 10.1021/acscatal.9b02347
ACS Catal. 2019, 9, 8509−8519